



Numerical Simulation of Local Scour around Underwater Pipeline based on FLUENT Software

Z. Zhang^{1,2,3†} and B. Shi²

¹*Zhejiang Institute of hydraulics and Estuary, Hangzhou, 310020, China*
²*College of Engineering, Ocean University of China, Qingdao, 266100, China*
³*Zhejiang Provincial Key Laboratory of Estuary and Coast*

†*Corresponding Author Email: 82457114zzy@163.com*

(Received March 6, 2014; accepted April 15, 2015)

ABSTRACT

This paper proposed a new methodology which was based on computational fluid dynamics for predicting the scouring process of underwater pipeline. By redeveloping a commercial CFD computer code, the governing equations for the flow model was solved by finite volume method and wall shear stress which acted as the key parameter to judge the incipient motion of sediment was firstly calculated. Then the morphological change of the sandy bed was simulated by dynamic mesh technology. Based on the comparisons between experimental results and numerical results, it was confirmed that present numerical modeling method can simulate the flow field and scouring process around underwater pipeline accurately. Besides, the influence of gap ratios on the scour behaviors was investigated by the present simulation.

Keywords: Underwater pipeline; Local scour; Numerical simulation; FLUENT; User defined function.

1. INTRODUCTION

Offshore pipeline, which transfers oil or gas from offshore to onshore, is one of the most important marine engineering equipment. As for the offshore pipelines laid directly on sandy seabed, the complex marine hydrodynamic conditions often induce the local scour and cause the suspension of pipeline, which makes the offshore pipeline unstable and have potential risk of fracture. At present, many researchers have studied the local scour around pipelines under currents by physical model tests and proposed different empirical equations describing the equilibrium scour depth of submarine pipeline respectively, such as (Mao Y.1986), (Sumer and Fredsøe1990), (Chiew1991), (Moncada and Aguirre 1999), (Yang *et al.*2012). Besides, numerical solution is also another efficient method to study the local scour around underwater pipeline. Brørs (1999) developed a scour model which considered the suspended sediment transport and bed-load sediment transport. (Li and Cheng1999, 2001) proposed a mathematical model to simulate the scour hole around offshore pipelines. This model assumed that the shear force at the bed surface was not larger than the critical shear force when scour reached to equilibrium state. (Liang *et*

*al.*2004) established a 2D numerical model to simulate the flow field and scour around offshore pipeline using finite difference method. (Lu *et al.*2007) simulated local scour around submarine pipelines based on the finite element method and unstructured triangle grid system. The equilibrium scour depth was obtained by this model. However, the scouring process could not be simulated using this model. (Zhao and Fernando 2007) employed an Eulerian two-phase model embedded in the FLUENT software to simulate the scour around pipeline. The simulation results certified the capability of simulating the temporal evolution of the scour profile and also found that the model over-predicted the sediment phase velocities under the water and the sediment interface within the bed. (Abbas *et al.*2011) used the Euler-Euler two phase model to simulate the tunnel erosion beneath underwater pipeline, however, the scouring process after the tunnel erosion was not simulated. (Zhang *et al.*2013) established a new numerical model to simulate the seepage flow by assuming the seabed as porous media and adding source terms in momentum equations. Using this model, they discussed the influence of impermeable plate below pipeline on the seepage flow under steady flow and gave the critical length of plate for preventing scour. The above numerical

studies show that the sediment transport model is more suitable for modeling the sediment scour than the two phase model.

FLUENT software is an advanced commercial CFD code. It can simulate the flow field of any case and shows good reliability. However, there is no sediment scour model in it and the scour process can not directly be simulated using this software. FLUENT software supplies a secondary development technology which is called user defined function (UDF). Using this function any complex models, such as moving items (Belkheir *et al.*2012) can be simulated. (Xiong *et al.* 2014) redeveloped the software and simulated the scour around pier, which shows that this software can be redeveloped to simulate the scour process. In this study a bed-load sediment transport equation dependent on relative wall shear force is derived and the sediment transport model is embedded into FLUENT. Deformation of the scour hole is captured using dynamic mesh technology. Based on this model, the influence of initial gap distance on flow field and scour behaviors around underwater pipeline is studied.

2. FLOW MODEL

2.1 Governing Equations

The governing equations for the flow around underwater pipeline are the continuity equation and the momentum equation which can be referred by (Zhang *et al.* 2013).

2.2 Turbulence Model

The $k-\epsilon$ turbulence model is one of the most common model used to predict the effects of turbulence.(Liang *et al.*2004) and (Xiong *et al.* 2014) used $k-\epsilon$ turbulence model to simulate the scouring process around pipeline and pier respectively and all got more accurate results than other turbulence model, such as Smagorinsky subgrid scale (SGS) model. Consequently, standard $k-\epsilon$ turbulence model was also used in this paper. The transport equations governing the turbulent kinetic energy k and its dissipation rate ϵ can be described as follows.

k equation:

$$\frac{\partial(\rho k)}{\partial t} + \frac{\partial(\rho k u_i)}{\partial x_i} = \frac{\partial}{\partial x_j} \left[\left(\mu + \frac{\mu_t}{\sigma_k} \right) \frac{\partial k}{\partial x_j} \right] + G_k - \rho \epsilon \quad (1)$$

ϵ equation:

$$\frac{\partial(\rho \epsilon)}{\partial t} + \frac{\partial(\rho \epsilon u_i)}{\partial x_i} = \frac{\partial}{\partial x_j} \left[\left(\mu + \frac{\mu_t}{\sigma_\epsilon} \right) \frac{\partial \epsilon}{\partial x_j} \right] + C_{1\epsilon} \frac{\epsilon}{k} G_k - C_{2\epsilon} \rho \frac{\epsilon^2}{k} \quad (2)$$

Where ρ =fluid density; u_i =velocity component along x_i direction; x_i =axis direction. ($i=1,2$); μ =fluid viscosity and μ_t = turbulent eddy viscosity; $C_{1\epsilon}$, $C_{2\epsilon}$, σ_k , σ_ϵ are the constants, and they are 1.44,1.92,1.0,1.03 respectively; G = generation of turbulence kinetic energy. Besides, the standard

wall function is implemented near the wall.

3. SEDIMENT TRANSPORT MODEL

3.1 Bed Load Transport

In this study the bed load sediment is considered. The model used here is similar to the model described by (Xiong *et al.*2014).With the increase of flow velocity, the shear force on sediment also increases and when the force exceeds the critical incipient shear force of sediment, the removal or transportation of sediment will occur.

For a flat sandy bed, the critical shear force of sediment incipient motion can be calculated as

$$\tau_{cr0} = \rho g (s - 1) d_{50} \theta_{cr0} \quad (3)$$

where τ_{cr0} =the critical shear force over flat sandy bed; g = the gravity acceleration; s = sediment specific weight; d_{50} =the mean sediment diameter; θ_{cr0} =critical shields number (dimensionless shear force) and can be obtained by the formula.

$$\theta_{cr0} = \frac{0.3}{1 + 1.2 D_*} + 0.055 [1 - \exp(-0.02 D_*)] \quad (4)$$

where $D_* = d_{50} [g(s-1)/\nu^2]^{1/3}$.

As for the sediment incipient on the slope, the critical shear force is adjusted to a higher threshold condition for sediment motion upslope and lower threshold condition down slope compared with the flat bed threshold θ_{cr0} , using the formula.

$$\tau_{cr} = \tau_{cr0} \left(\cos \alpha + \frac{\sin \alpha}{\tan \varphi} \right) \quad (5)$$

where α is slope angle of sandy bed, φ is repose angle of the sediment.

The sediment transport rate formula described by Souls by is chosen for this model.

$$q_0 = 12 \sqrt{g (s - 1) d_{50}^3 \theta (\theta - \theta_{cr})} \quad (6)$$

where q_0 is the bed load sediment transport rate per unit width over a flat bed.

The bed load sediment transport rate at the slope will be adjusted according to the formula

$$q_{bi} = q_0 \frac{\tau_i}{|\tau|} - C q_0 \frac{\partial h}{\partial x_i} \quad (7)$$

where τ_i is the shear force at x_i direction. The second term is a slope correction term. Laboratory measurements indicate that C is in the range of 1.5-2.3, and $C=1.5$ is used in the present study. h is the sandy bed level.

According to the theory of mass balance of sediment transportation, the change of bed level h can be expressed as

$$\frac{\partial h}{\partial t} = \frac{-1}{(1-n)} \left(\frac{\partial q_{bi}}{\partial x_i} \right) \quad (8)$$

Where n is porosity of sediment.

4. DYNAMIC MESH TECHNOLOGY

The sandy bed boundary's motion is decided by the interaction with the water around it. Sandy bed's shear forces are obtained from the CFD solver's solution of last time step and used to calculate the boundary nodes' new positions by the sediment transport model. In order to move the sandy bed boundary, the equation of motion is written as a DEFINE_GRID_MOTION UDF which is embedded into FLUENT. After the boundary's refreshing, the finite volume mesh also needs to be updated. The automatic mesh deformation is implemented by a Laplacian smooth operator (Liu and Marcelo 2008).

5. NUMERICAL SOLUTION AND BOUNDARY CONDITIONS

As for the flow model, the governing equations are discretized by finite volume method. For pressure-velocity coupling, the SIMPLE scheme is used in this model. The sediment transport model is written as a user defined function in FLUENT. The bed change equation (Eq.8) is solved using finite difference method.

The computational domain is a vertical 2D domain (Fig.1). The velocity inlet boundary is used for the upstream boundary. The boundary conditions are defined as

$$u(z) = \min \left\{ \frac{u_*}{\kappa} \ln \left(\frac{z}{z_0} \right), u_0 \right\} \quad (9)$$

$$k(z) = \max \left\{ C_\mu^{-1/2} \left(1 - \frac{z}{\delta} \right)^2 u_*^2, 0.0005 u_0^2 \right\} \quad (10)$$

$$\varepsilon(z) = \frac{C_\mu^{3/4} k(z)^{3/2}}{l(z)} \quad (11)$$

$$l(z) = \min \left\{ \frac{\kappa z}{1 + 1.5z/\delta}, C_\mu \delta \right\} \quad (12)$$

The friction velocity is evaluated as $u_* = \kappa u_0 / \ln(\delta/z_0)$, δ is the water depth in this model. For the bed roughness length, z_0 can be defined as $2.5d_{50}/30$. The von Karman constant κ is 0.4.

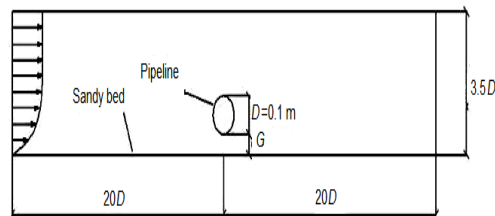


Fig.1. Computational domain.

Outflow boundary is applied at the outlet boundary. The wall boundary condition as well as a standard wall function is used at the water-sediment interface. The water surface's change is neglected. The computational domain is discretized with non-

structured 2D cells.

6. PHYSICAL EXPERIMENT

6.1 Experiment Setup

The experiments were carried out in an annular flume which is 25.0 m long, 0.5 m wide and 0.6 m deep (Fig.2). Part of flume was filled with sediment, which represented the sandy bed. The other side was a fixed bed, which was at the same level as the sandy bed. One tested pipe was laid above the sandy bed to study the scour process and the other pipe was laid on the fixed bed to study the flow characteristics. The diameters of the tested pipes investigated in experiments were $D=0.1$ m. The initial gap distance between pipe and sandy bed can be adjusted by vertical sliding support. The sandy bed was of 0.15m height in the flume. The sand used here is noncohesive with a median size of $d_{50}=0.3$ mm and a porosity $n=0.5$, the repose angle of the sediment is $\phi=32^\circ$, the critical Shields number for a horizontal bed is 0.038. A high accuracy instrument ADV (Acoustic Doppler velocimetry) was selected to measure the velocity across four cross sections at various gap ratios (Fig.3). Besides, each case in this experiment lasted 150 minutes to get the equilibrium scour depth.

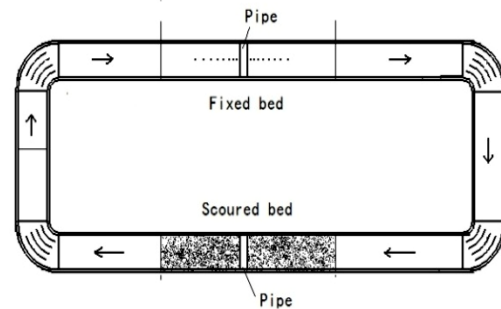


Fig.2. Layout of physical model.

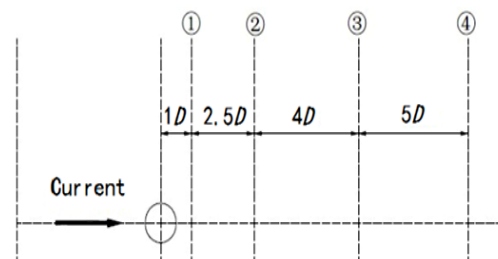


Fig.3. Positions of velocity cross sections.

6.2 Experiment Parameters

In the experiment, the experiment cases with different gap ratios ($G/D=0.0, 0.1, 0.3$ and 0.5) on both fixed bed and scoured bed were investigated (Table1). The inflow velocity was 0.25m/s and the water depth was kept as constant of 0.35m. The experimental parameters were listed in Tab.1.

Table1 Experimental parameters

| Bed type | Case No. | Pipe diameter (m) | Velocity (m/s) | Gap ratio (G/D) |
|-------------|----------|-------------------|----------------|-----------------|
| Scoured bed | 1 | 0.1 | 0.25 | 0.0 |
| Scoured bed | 2 | 0.1 | 0.25 | 0.1 |
| Scoured bed | 3 | 0.1 | 0.25 | 0.3 |
| Scoured bed | 4 | 0.1 | 0.25 | 0.5 |
| Fixed bed | 5 | 0.1 | 0.25 | 0.0 |
| Fixed bed | 6 | 0.1 | 0.25 | 0.1 |
| Fixed bed | 7 | 0.1 | 0.25 | 0.3 |
| Fixed bed | 8 | 0.1 | 0.25 | 0.5 |

7. RESULTS AND DISCUSSIONS

7.1 Flow Structure

As for the flow around pipe, the flow structure at $G/D=0$ is different from other cases. (Mao Y. 1986) found that there are three vortexes in case of $G/D=0$. Present numerical and experimental results also certified his viewpoint. Fig.4 shows the flow streamlines around pipe with no gap between pipe and wall. It can be seen that there are a larger clockwise vortex B behind the pipe and two smaller vortexes A and C both in front of and behind the pipe near the wall. The vortexes A and C may induce the sediment suspension and hence cause the occurrence of scour tunnel. Fig.5 shows the typical flow structures when $G/D=0.1, 0.3$ and 0.5 . Three cases all present vortex shedding phenomenon which is not seen in case of $G/D=0$. However, because of the wall's influence, the interaction between the underneath shear layer and external layer in wake flow region is blocked, which prevents the increase of vorticity. Consequently, the vortex below is not fully developed and its size is smaller than above one in case of $G/D=0.1$ and 0.3 . In case of $G/D=0.5$, the wall's influence decreases and both vortexes are nearly kept as the same size.

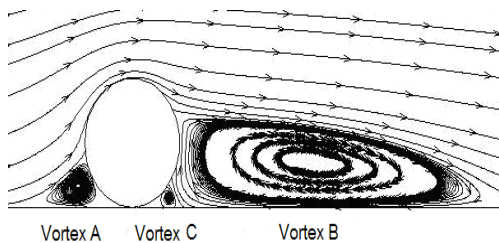
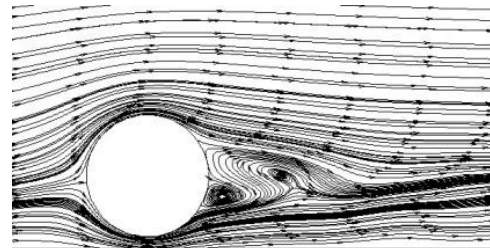


Fig. 4. Flow pattern around the pipeline when $G/D=0$.

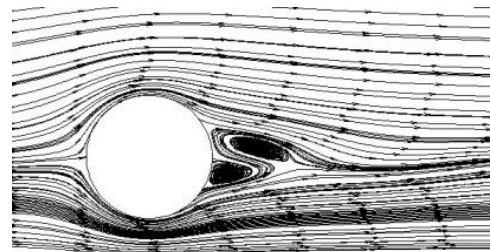
7.2 Velocity Distribution

Due to the different flow structures with or without gap between pipe and wall, the velocity distributions are also different. Fig.6 and Fig.7 listed experimental and numerical results of the horizontal velocity at four cross sections when gap ratio equals 0.0 and 0.3 respectively and the velocity distribution at $G/D=0.1$ and 0.5 are similar with $G/D=0.3$, which are not shown here. Seen from Fig.6, it can conclude that due to the blockage of pipe, at $x=1.0D$, the velocity above the top of pipe is larger and there is a sharp decrease with the height

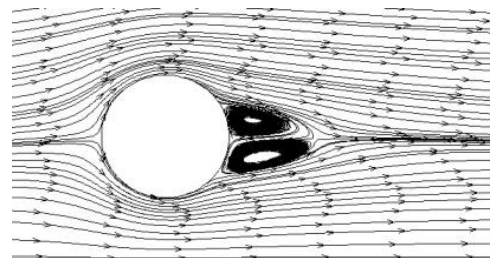
decreasing from $1.4D$ to $0.8D$. There is a backflow below $x=0.5D$ and the velocity is small. At $x=3.5D$, the backflow velocity is larger than the velocity at $x=1.0D$ while the shear flow region becomes larger. At $x=7.5D$ cross section which locates at the end of vortex B, there is nearly no backflow below the region of $z=1D$. The flow velocity increases with the increasing height. With the increasing distance away from the pipe, the influence of pipe becomes insignificant and the velocity gradually returns to the incoming velocity distribution, which has been verified by the velocity distribution at $x=12.5D$.



(a) $G/D=0.1$



(b) $G/D=0.3$



(c) $G/D=0.5$

Fig.5. Flow patterns at various gap ratios.

As for the flow around pipe with a gap, flow separates from the pipe surface at two sides, leading to the generation of wake flow. An S-shape velocity profile is found at the cross sections of $x/D=1$ and $x/D=3.5$. Section of $x/D=1$ is in the lee-wake region and the negative velocity indicates the presence of the vortex. No backflow is found at the section of $x/D=3.5$, indicating that the vortex disappears at that distance away from the pipeline. At $x/D=7.5$, the flow distribution nearly returns to its initial state. Fig.6 and Fig.7 also show that the numerical results are in agreement with experimental results, especially the velocity near the bed, which lays the foundation for simulating the scouring process accurately.

7.3 Scour Characteristics

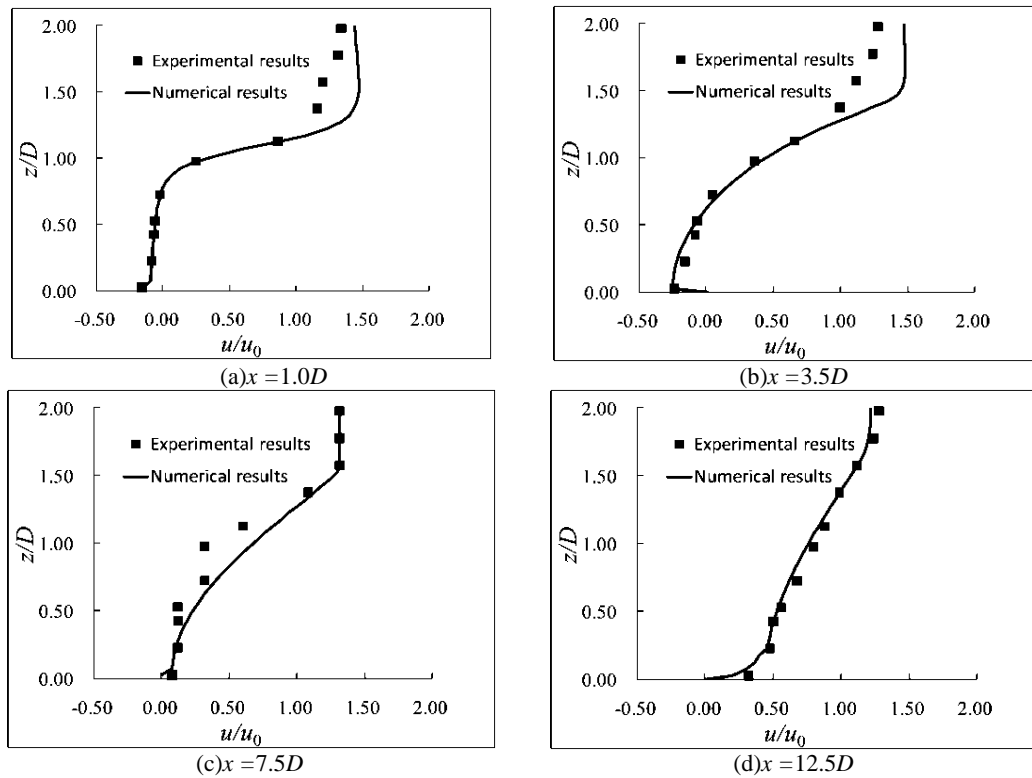


Fig. 6. Velocity distributions in case of $G/D=0.0$.

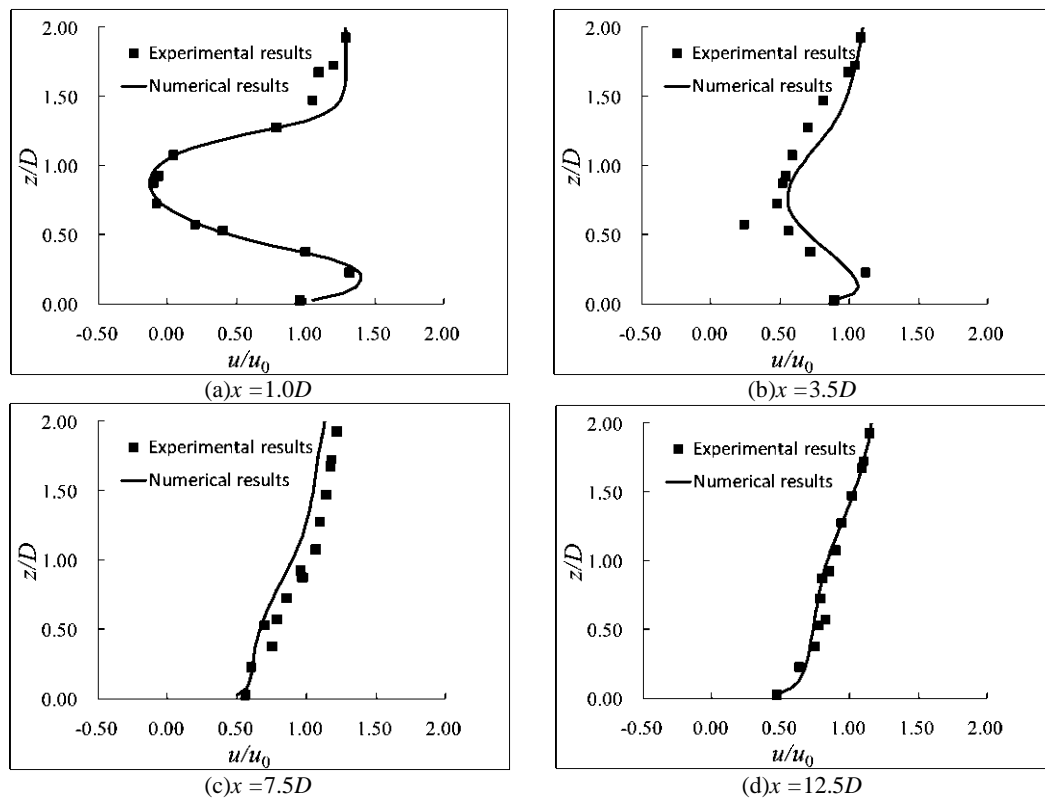


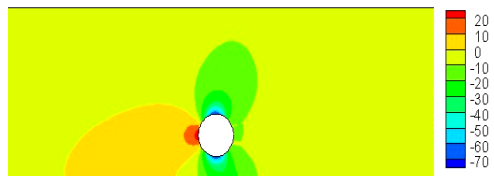
Fig. 7. Velocity distributions in case of $G/D=0.3$.

In this study, the evolution of the scour hole in case of $G/D=0.5$ was selected to illustrate the scouring

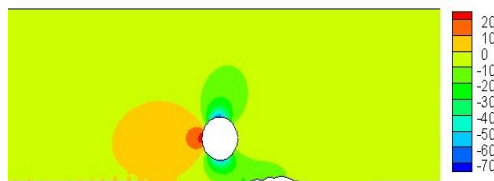
process. Fig.8 shows the pressure fields around scouring bed at different times. With the change of

bed level, the pressure changes correspondingly. When $t=150$ min, the pressures along the sandy bed underneath the pipeline are larger than those in previous time, and the pressures on the bottom of pipeline also increase more clearly than other positions of the pipeline.

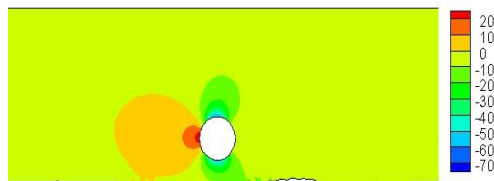
The sandy bed's scouring process can also be observed in Fig.8. From $t=0$ min to $t=5$ min, the scouring process is similar with the scour caused by horizontal jet. The scour hole changes from shallow to deep upstream with the extension of dune downstream increases. And at this early stage, the scouring is vigorous. After the initial scouring process, the dune is moved towards downstream by flow, and the scour hole changes slowly. From $t=30$ min to 150 min, the scour hole has a smaller change, and the dune nearly disappears. When $t=150$ min, the profile of sandy bed is in agreement with the scour hole which is shown in Fig.9 in experiment.



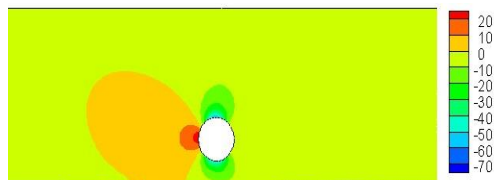
(a) $t=0$ min



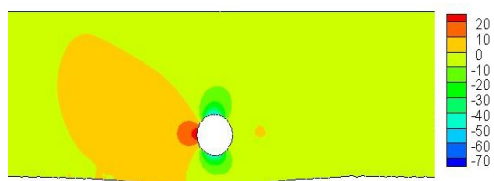
(b) $t=1$ min



(c) $t=5$ min



(d) $t=30$ min



(e) $t=150$ min

Fig.8. Pressure (Unit: Pa) distributions at different times.

The scouring processes at other gap ratios except $G/D=0.0$ are similar to the case of $G/D=0.5$. In case of no gap, the scouring is caused by the seepage piping which cannot be simulated by present numerical model at early pipeline. And after the appearance of flow tunnel between pipeline and sandy bed, the scouring will go on due to flow. The equilibrium scour holes in all cases are shown in Fig.10. The scour profiles are similar in four different cases in the experiment, as well as for the two cases ($G/D=0.3$ and 0.5) in the simulation using the same sand and velocity. The agreement between numerical results and experimental results at various gap ratios validates the mathematical model's accuracy. It can also be observed that the maximum scour depth decreases with the increasing of initial gap ratio.

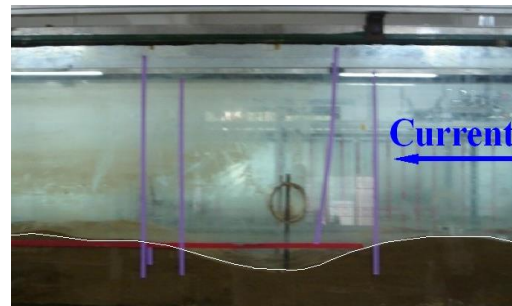


Fig.9. Scour hole in experiment when $t=150$ min ($G/D=0.5$).

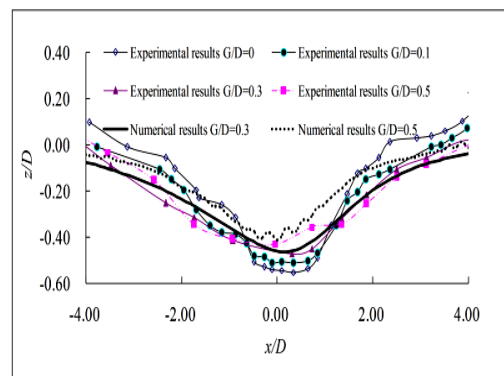


Fig.10. Equilibrium scour profiles at various gap ratios.

The equilibrium scour depths in different cases in this study are shown with previous ones in Fig.11. Note that there are some differences between the present conditions and previous ones. It can be observed that the experimental results are a little deeper than numerical results, and the variation rule of equilibrium scour depth versus initial gap ratio is linear. The equilibrium scour depth at various gap ratios can be obtained as follows:

$$S = S_0 - m(G / D) \tag{13}$$

Where S_0 is the equilibrium scour depth when there is no gap between pipeline and sandy bed, and m is correlation coefficient. The correlation coefficient m is 0.29 by data fitting, indicating that the fitted curves (Fig.11) agree well with the scatters and Eq.13 can be used as a semi-empirical formula to

describe the equilibrium scour depth at various initial gap ratios.

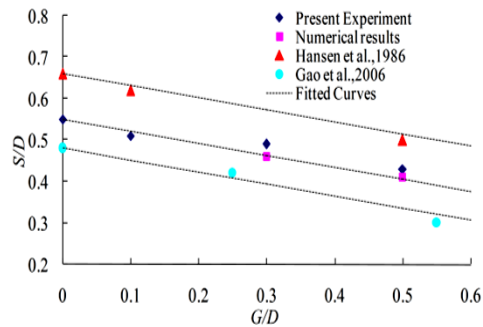


Fig.11. Equilibrium scour depth versus initial gap ratio.

8. CONCLUSIONS

The clear-water scour below underwater pipeline is simulated using finite volume method and dynamic mesh. A sediment model that only considers bed load sediment is established using user defined function in FLUENT, in which the Shields number is the major parameter. The new sediment model is then used to simulate the bed deformation around underwater pipeline. The main conclusions can be summarized as follows.

The comparisons between the experimental results and numerical results show that the mathematical model can simulate the process of local scour below underwater pipeline well and can obtain equilibrium profiles which are similar to the experimental results.

On condition of the same sandy bed and flow velocity, the scour holes show geometric similarity at various initial gap ratios. The clear-water scour equilibrium depth decreases with the increasing gap ratio, and the semi-experience formula is proposed according to computational and experimental results.

ACKNOWLEDGEMENTS

The authors would like to acknowledge the financial supports from the National Nature Science Fund of China (Grant No. 41376099, 51279189), the Zhejiang Province Science and Technology Conditions of Construction Project(2016C33086).

REFERENCES

Abbas, Y. B., H.K. Mohammad, E.S. Amir, H.B. Jaco and L. Cheng (2011). Euler–Euler two-phase flow simulation of tunnel erosion beneath marine pipelines. *Applied Ocean Research* 33(2), 137-146.

Belkheir, N., R. Dizene and S. Khelladi (2012). A Numerical Simulation of Turbulence Flow around a Blade Profile of HAWT Rotor in Moving Pulse. *Journal of Applied Fluid Mechanics* 5(1), 1-9.

Brørs, B. (1999). Numerical Modeling of Flow and Scour at Pipelines. *Journal of Hydraulic Engineering* 125(5), 511-523.

Chiew, Y.M. (1991). Prediction of maximum scour depth at submarine pipelines. *Journal of Hydraulic Engineering* 117(4), 452-466.

Gao, F.P., B. Yang, Y. X. Wu and S. M. Yan (2006). Steady current induced seabed scour around a vibrating pipeline. *Applied Ocean Research* 28(5), 291-298.

Hansen, E.A., J. Fredsøe and Y. Mao (1986). Two-dimensional scour below pipelines. *Proceedings of the Fifth International Symposium on Offshore Mechanics and Arctic Engineering*, New York 670-678.

Huai, W.X., Z. W. Wang, Z. D. Qian and Y. Q. Han (2011). Numerical simulation of sandy bed erosion by 2D vertical jet. *Science China: Technological Science* 54(12), 3265-3274.

Li, F. and L. Cheng (1999). A numerical model for local scour under offshore pipelines. *Journal of Hydraulic Engineering* 125(4), 400-406.

Li, F. and L. Cheng (2001). Prediction of lee-wake scouring of pipelines in currents. *Journal of Waterway, Port, Coastal and Ocean Engineering* 127(2), 106-112.

Liang, D.F., L. Cheng and F. Li (2004). Numerical modelling of scour below a pipeline in currents. part: Scour simulation. *Coastal Engineering* 52(1), 43-62.

Liu, X.F. and H. G. Marcelo (2008). Three-Dimensional Numerical Model with Free Water Surface and Mesh Deformation for Local Sediment Scour. *Journal of Waterway, Port, Coastal and Ocean Engineering* 134(4), 203-217.

Lu, L., Y. C. Li and J. M. Qin (2007). Numerical simulation of the equilibrium profile of local scour around submarine pipelines based on renormalized group turbulence model. *Ocean Engineering* 32(17), 2007-2019.

Mao, Y. (1986). *The interaction between a pipeline and an erodible bed*. Denmark: The Technology University of Denmark.

Moncada, M.A. and J. Aguirre-Pe (1999). Scour below pipeline in river crossings. *Journal of Hydraulic Engineering* 125(9), 953-958.

Qi E.R., G. Y. Li, W. Li, J. Wu and X. Zhang (2006). Study of vortex characteristics of the flow around a horizontal circular cylinder at various gap-ratios in the cross-flow. *Journal of Hydrodynamics, Ser. B*, 18(3), 334-340.

Sumer, B.M. and J. Fredsøe (1990). Scour below pipelines in waves. *Journal of Waterway, Port, Coastal and Ocean Engineering* 116(3), 307-323.

Z. Zhang and B. Shi /*JAFM*, Vol. 9, No. 2, pp. 711-718, 2016.

- Xiong, W., C. Cai and B. Kong (2014). CFD Simulations and Analyses for Bridge-Scour Development Using a Dynamic-Mesh Updating Technique. *Journal of Computing in Civil Engineering*, 10.1061/(ASCE)CP.1943-5487.0000458.
- Yang, Z.D. (1996). Sediment transport : Theory and Practice. New York: The McGraw-Hill Companies.
- Yang, L.P., B. Shi, Y.K. Guo and X.Y. Wen (2012). Calculation and experiment on scour depth for submarine pipeline with a spoiler. *Ocean Engineering* 55(1), 191-198.
- Zhang, Z.Y., B. Shi, Y. K. Guo and L. P. Yang (2013). Numerical Investigation On Critical Length of Impermeable Plate Below Underwater Pipeline Under Steady Current. *Science China: Technological Sciences* 56(5), 1232-1240
- Zhao, M. and L. Cheng (2008). Numerical modeling of local scour below a piggyback pipeline in currents. *Journal of Hydraulic Engineering* 134(10), 1452-1463.
- Zhao, Z.H. and H. J. S. Fernando (2007). Numerical simulation of scour around pipelines using an Euler-Euler coupled two-phase model. *Environment Fluid Mechanics* 7(2), 121-142.
- Zhu, Z.W. and Z. Liu (2012). CFD prediction of local scour hole around bridge piers. *Journal of Central South University of Technology* 19(1), 273-281.